Modeling the competition between elastic and plastic relaxation in semiconductor heteroepitaxy: From cyclic growth to flat films

Fabrizio Rovaris, Roberto Bergamaschini, and Francesco Montalenti*
L-NESS and Department of Materials Science, University of Milano-Bicocca, Via R. Cozzi 55, I-20125 Milano, Italy
(Received 15 June 2016; revised manuscript received 19 October 2016; published 16 November 2016)

We introduce a continuum model of deposition and surface diffusion tackling semiconductor heteroepitaxy also in the presence of misfit dislocations. During the evolution defects are inserted on the fly whenever their presence lowers the energy of the system, and the corresponding stress field is added to the one produced by lattice mismatch. An application to Ge/Si is provided. The wealth of qualitatively different behaviors experimentally reported in the literature is reproduced.

DOI: 10.1103/PhysRevB.94.205304

I. INTRODUCTION

In the presence of a lattice mismatch between substrate and deposited material, coherent films experience a biaxial stress. As the film volume increases, elastic energy accumulates until relaxation sets in. There exist two qualitatively different paths leading to misfit-strain relief. Three-dimensional (3D) islands can be formed, partially relaxing the in-plane strain owed to the exposure of facets. This is the path followed by systems displaying the Stranski-Krastanow (SK) growth mode after completion of a wetting layer (WL). Systems of major technological interest, such as InGaAs/GaAs or Ge/Si display SK behavior so that the dynamics of WL + islands formation was widely investigated and several reviews on the subject exist (see Refs. [1–4] for recent ones). The stress load can alternatively be diminished by misfit-dislocation injections. Relaxation via dislocations in heteroepitaxial films is also a very popular topic (see Ref. [5] for a review). This is not surprising as control over defects is one of the key steps needed to develop high-performance devices.

Under usual deposition conditions, elastic relaxation precedes dislocation formation in both InGaAs/GaAs(001) [6] and Ge/Si(001) [7]. Some applications benefit from a planar morphology of the film so that research was devoted to triggering plastic relaxation before SK islands are formed. At present, a popular working recipe involves a low-temperature deposition phase [8,9], inhibiting lateral collection of adatoms, therefore hindering island formation. The onset of plastic vs elastic relaxation can therefore be controlled by suitably tuning the growth parameters.

Experimental evidence by LeGoues *et al.* [10], dating more than 20 years ago, has shown the fascinating peculiarity of heteroepitaxial-growth dynamics under the simultaneous effect of the two phenomena. By *in situ* electron microscopy, the authors showed oscillations in island shapes, attributed to successive insertion of misfit dislocations in SK Ge islands on Si(001). Besides the dramatic evidence of such cyclic growth supplied in Ref. [10] (but see Ref. [11] for a previous report), the influence of dislocations on SK islands has been inferred by simple height-to-base aspect ratio (AR) vs volume (V) plots. As highlighted in several papers [12–14], the onset of plasticity is signaled by a transition beyond a critical volume from a monotonous AR increase vs V to a less well-defined (due to fluctuations) behavior, almost a plateau.

From a qualitative point of view it is easy to picture the main consequences of introducing a misfit dislocation inside a coherent island. High ARs allow for strong strain relaxation but require a large cost in terms of surface energy (see, e.g., Ref. [2]). Insertion of a dislocation within an island lowers the need for strain relaxation so that a flatter configuration becomes energetically favorable. Static calculations investigating the onset of plasticity and the shape of dislocated islands have been reported in several papers [10,14,15], noticeably including Ref. [16] where oscillations in the AR were predicted. However, a deep understanding of the process can be reached only by a full dynamical simulation, describing the system behavior during growth without any *a priori* knowledge of the island shape or of the dislocation distribution.

In this paper, starting from a standard continuum growth model based on surface diffusion, we propose an extension allowing for a direct treatment of the role played by misfit dislocations. Defects are introduced on the fly during the system evolution, based on a suitable energetic criterion. Results are compared with several experimental data from the literature.

The paper is organized as follows. In Sec. II relevant details of the model are described. Simulation results follow in Sec. III where two possible regimes of growth are identified. Section III A describes growth of heteroepitaxial islands in a quasiequilibrium regime, providing the evidence of cyclic growth. Section III B instead deals with out-of-equilibrium growth conditions, leading to plastically relaxed flat films, by kinetic suppression of islanding. Conclusions and final remarks are reported in Sec. IV.

II. METHOD

A. Model definition

In this paper we investigate the dynamics of heteroepitaxy in the most complex scenario, involving competition between elastic and plastic relaxation. To this goal we exploit a two-dimensional (2D) continuum model in which the dynamics results from the combined effect of deposition and surface diffusion driven by the thermodynamic tendency toward free-energy minimization, i.e., material moves against the

*francesco.montalenti@unimib.it

 ©2016 American Physical Society

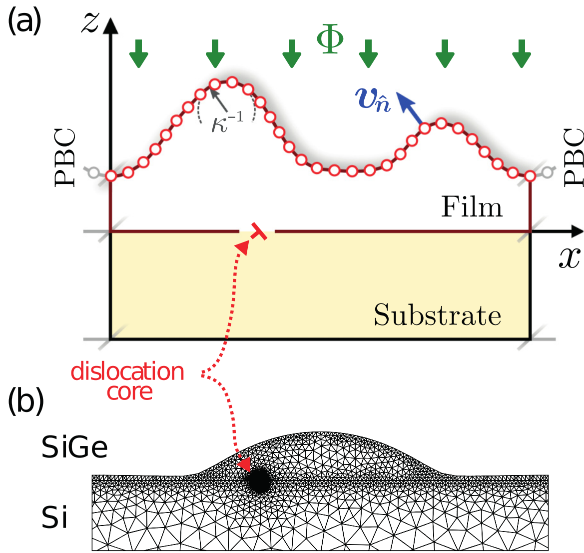

FIG. 1. Model schematics. (a) Simulation cell as defined from the $z(x)$ surface profile. (b) Example of locally refined mesh used in the simulations. The region near the defect cores is finely refined in order to better describe the high variation in the stress/strain field close to dislocations.

local gradients of the chemical potential μ. Bulk diffusion is negligible at the typical growth temperatures due to high activation barriers [17]. At each time t, the profile evolution is defined by a local velocity $v_{\hat{\boldsymbol{n}}} = -\boldsymbol{\Phi} \cdot \hat{\boldsymbol{n}} + M\nabla_S^2\mu$ tracing the motion of each point of the profile in the direction of the surface normal $\hat{\boldsymbol{n}}$ (the subscript S indicates that gradients are to be evaluated along the surface coordinate). M is a mobility coefficient, setting the time scale for the evolution. Deposition is assumed as a vertical flux $\boldsymbol{\Phi} = -\Phi\hat{z}$, mimicking typical molecular-beam epitaxy conditions.

An explicit description of the film profile is here considered in 2Ds as sketched in Fig. 1. The height function $z = z(x)$ traces the local film thickness with respect to the film/substrate interface (at $z = 0$). Periodic boundary conditions (PBCs) are assumed. In a small slope approximation, the evolution for the profile is obtained by projecting the net material flux along the vertical direction,

$$\frac{\partial z}{\partial t} = \Phi + M\frac{\partial}{\partial x}\left[\frac{1}{\sqrt{1+z'^2}}\frac{\partial \mu}{\partial x}\right], \tag{1}$$

where the prime means differentiation with respect to x. Once defined μ, the evolution is determined by integrating in time Eq. (1).

The system free-energy F comprises three major contributions: surface, wetting, and elastic energy. Correspondingly, the chemical potential (per unit volume) takes the form

$$\mu = \frac{\delta F}{\delta z} = \kappa\gamma + \frac{1}{\sqrt{1+z'^2}}\frac{d\gamma}{dh} + \rho. \tag{2}$$

The first term accounts for the cost of exposing free surfaces, and for isotropic surface energy density γ, it is proportional to the local profile curvature κ. The second term accounts for film/substrate wetting [18,19], here assumed as resulting from the dependence of γ on the film thickness. In agreement with *ab initio* calculations in literature [20,21]: $\gamma(h) = \gamma_f + (\gamma_s - \gamma_f)\exp(-h/\delta)$ with γ_f and γ_s as the surface energy density for the film and substrate material, respectively, and δ as a decay length (typically a few atomic layers). The last contribution in Eq. (2) corresponds to the elastic energy density ρ at the surface, calculated in the assumption of mechanical equilibrium, within the linear elasticity theory for an isotropic medium, resulting from both misfit strain and dislocations.

Analytic functions are known for the strain field induced by dislocations in the bulk of a crystal [22] and for the case of a perfectly flat film [23–25]. When considering a generic surface profile as in the present case, no general solution is available, and mechanical equilibrium must be explicitly solved by a numerical approach. To this goal, it is convenient to resort to the formalism of eigenstrains [26] by defining

$$\varepsilon^*_{ij} = f\delta_{ij} + \varepsilon^{\mathrm{d}}_{ij}, \tag{3}$$

where f is the lattice misfit and $\boldsymbol{\varepsilon}^{\mathrm{d}}$ is the permanent deformation induced by the dislocations. The total strain is then $\varepsilon_{ij} = (1/2)(\partial u_i/\partial x_j + \partial u_j/\partial x_i) - \varepsilon^*_{ij}$ with $\boldsymbol{u}$ as the local displacement.

In principle, $\boldsymbol{\varepsilon}^{\mathrm{d}}$ should be defined as the unrelaxed displacement field imposed by the dislocations [27,28]. However, here, we find more convenient to follow the approach discussed in Refs. [29,30] setting the eigenstrain as the initial approximated solution provided by the analytic functions available for arrays of dislocations [22] as required by PBCs. A dipole construction is also exploited to suppress spurious lateral interactions resulting from the long-range r^{-1} dependence of the dislocation strain field. Furthermore, the stress field in the proximity of the dislocation core is regularized by exploiting the convenient procedure suggested in Ref. [31] in order to avoid numerical divergence (this is especially needed in order to integrate the elastic energy).

The introduction of dislocations into the system is performed on the fly during the growth simulation. In particular, the variation in the total elastic energy is probed by placing the dislocation at different sites along the film/substrate interface. In case a position leading to energy lowering is found, the dislocation is placed there, and the corresponding stress field (see Ref. [29]) is added to the purely elastic one. The procedure is illustrated in Fig. 2. An extensive comparison between theory and experiments has shown that adding dislocations based on energy reduction is well justified in typical SiGe/Si(001) islands [15,29]. When dealing with flat films, instead, kinetic effects are expected to become important at small misfits ($f < 0.02$ [32]), a case not treated here, calling for a proper extension of the present model.

B. Computational details

A MATLAB code was developed for the numerical solution of the coupled PDEs for the profile evolution and the strain field at each time step. An explicit forward-Euler scheme is adopted for the time integration. A finite-element method subroutine, adapted from the code in Ref. [33], is exploited to solve the equation of mechanical equilibrium in the presence of both lattice misfit and dislocations.

The film free surface is interpolated from the discretized $z = z(x)$ profile, and the domain is partitioned into an

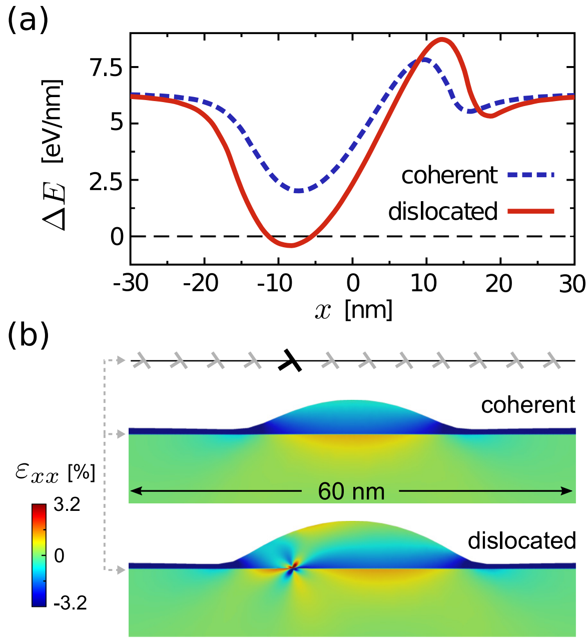

FIG. 2. During the evolution of the film profile, lateral scans are performed to check whether the presence of a further dislocation lowers the energy of the system ($\Delta E < 0$). All panels refer to the introduction of the first dislocation. (a) Energy difference between the system with and without dislocation for a small (dashed curve) and a large island (continuous line). (b) Morphology of the two islands and corresponding ε_{xx} strain map, including the effect of the dislocation for the larger one.

unstructured triangular mesh, built by an octree algorithm. As illustrated in Fig. 1(b), space adaptivity is exploited to optimize the computational costs. A high refinement level is imposed on a circular region around each defect to provide a better resolution of the dislocation field [29]. Also meshing at the film free surface and at the film/substrate interface is better refined with respect to the inner regions of both the film and the substrate.

Strain is computed as for a three-dimensional system where the actual 2D geometry (defined on the xz plane) is infinitely extended in the omitted (y) direction. Dislocations are positioned at the film/substrate interface with the dislocation line along such direction. A thick substrate region is included below the film to avoid spurious effects from the substrate bottom, where zero displacement is assumed.

The time scale of the simulation is left in arbitrary units and can be adapted to the experimental time scales by setting the value of the mobility constant M. Tentatively, M can be estimated from the diffusion coefficient $M = h_l V_a D_0 (kT)^{-1} \exp[E_b/(kT)]$ with h_l as the thickness of a monolayer, V_a as the volume per atom, D_0 as the material diffusion coefficient, E_b as the energy barrier for site hopping, k as the Boltzmann constant, and T as the temperature. Typical values for the Ge/Si system can be set as $h_l = 0.146$ nm, $V_a = 0.02$ nm^3, $D_0 = 8.5 \times 10^8$ nm^2/s [34], $E_b = 1.1$ eV [35], and a typical growth temperature of $T = 650\,^\circ$C is assumed, yielding a typical length scale for the simulated dynamics of the order of minutes. Notice that, in the presence of deposition, the evolution is entirely defined by the Φ/M ratio.

All simulations here reported were run by setting parameters for $Ge_{0.8}Si_{0.2}$/Si(001) [36]. In particular, the Young modulus (Poisson ratio) was set equal to 108 GPa (0.262) in the film and to 130 GPa (0.27) in the substrate, whereas a lattice misfit $f = 0.032$ was imposed. A 50-nm-thick substrate is assumed. Surface energy terms were set to $\gamma_f = 6.5$ eV/nm^2, $\gamma_s = 8.7$ eV/nm^2, and $\delta = 0.18$ nm, based on Ref. [20]. The ratio M/Φ was set equal to 10^4 when considering close-to-equilibrium conditions and decreased to 10^2 for simulations far from equilibrium.

III. RESULTS AND DISCUSSION

A. Island growth with dislocations

Simulation results corresponding to quasiequilibrium growth are displayed in Fig. 3. Film profiles at different times are shown, starting from the stage where our automatic procedure first leads to insertion of a dislocation. Previous stages, including WL formation, onset of the Asaro-Tiller-Grinfeld (ATG) instability [37,38], and coarsening, are not reported as the evolution in the absence of defects has already been widely discussed in the literature (see, e.g., Ref. [19]). Following Ref. [15], we considered only 60° dislocations, whose lowest-energy positions are laterally displaced with respect to the island center [15]. As a result only one side of the island strongly benefits from plastic relaxation. Thus, a second defect is quickly added to the other side as evidenced in panel (b). Then, the system evolves for a significant time without introducing further dislocations. As the chemical potential of the defected island is much lower with respect to the one of the coherent islands, coarsening is observed, the dislocated island enlarging at the expenses of

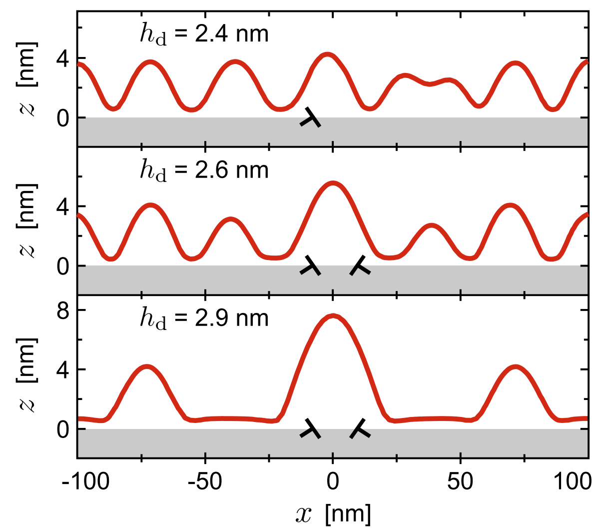

FIG. 3. Temporal evolution of the film profile for different amounts of material deposition h_d (directly proportional to time), corresponding to the injection of the first ($h_d = 2.4$ nm) and second ($h_d = 2.6$ nm) dislocation and to a later stage ($h_d = 2.9$ nm) where the island hosting the dislocations has quickly grown while the two adjacent coherent islands disappear.

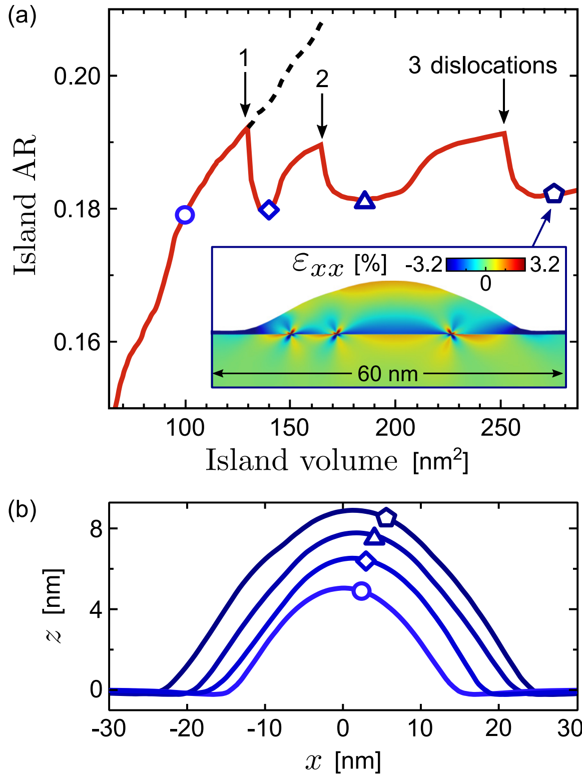

FIG. 4. (a) Evolution of the island AR as a function of the deposited material (directly proportional to time). A sharp change in behavior is seen when the first dislocation is introduced. From this stage the evolution substantially deviates from the corresponding one obtained by suppressing the injection of defects (dashed curve). The inset: strain map (ε_{xx} component) at the latest stage of evolution. (b) Island profiles recorded during the evolution at the stages marked by symbols in panel (a).

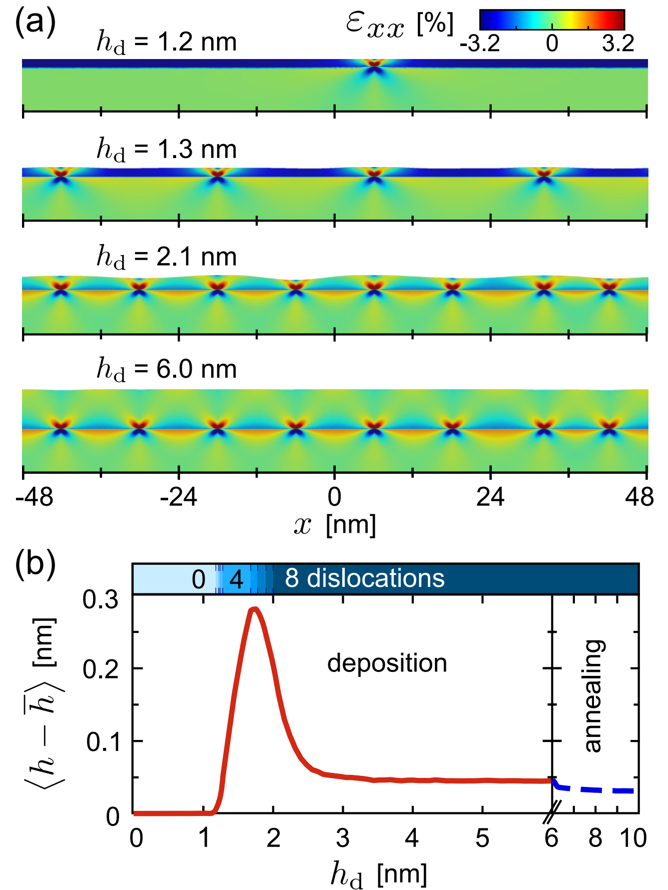

FIG. 5. (a) Relevant simulation stages for the evolution observed during out-of-equilibrium growth. Undulations are caused by the underlying dislocations. When full plastic relaxation is achieved the film becomes flat again. (b) Temporal evolution of the film roughness evidencing the onset of undulations, disappearing with increasing thickness. Once dislocated, the film is stable against annealing as shown by the simulation continuation without deposition (dashed line on the right). The number of dislocations is reported in the top colored bar.

the two lateral ones which disappear. The presence of large plastically relaxed islands surrounded by a depletion zone was clearly reported in several experiments (see, e.g., Fig. 1 of Ref. [13]).

Let us now follow the long-time evolution of a single dislocated island surrounded by a flat substrate. As more material is deposited, the island keeps on growing, and dislocations are added each time a critical-volume condition is met. The full development of the island is conveniently followed by the AR vs V curve reported in Fig. 4. Until the island is coherent, the AR grows with V as expected from simple static models [39]. When the first dislocation is introduced, the behavior changes. A sudden drop in the AR is observed: The effective lattice mismatch in the island is lowered, and flattening occurs to reduce the exposed surface. As the volume increases, however, the tendency towards increasing the AR to better release the strain dominates again, until a new dislocation is introduced. Our simulation predicts an oscillatory behavior of the AR and, thus, cyclic growth [see also the reported profiles in Fig. 4(b)]. This sudden change in behavior in the AR vs V curve has been reported in several experiments [12–14]. Actual oscillations are compatible with the observations, despite not being evident in curves derived from experiments due to the scatter among measures on several islands. The *in situ* observations by LeGoues *et al.* [10], however, leave little doubt on the presence of shape oscillations. Notice that islands' profiles in the presence of an odd number of dislocations are typically nonsymmetric [panel (b)] as a direct consequence of the strain field [inset in panel (a)]. The lack of lateral symmetry of some dislocated islands is quite evident in the experimental results of Ref. [13].

Despite the nice qualitative agreement with the experiments, our simulations seem to underestimate by ~30% the typical AR beyond which dislocations are inserted [13]. Further refinements needed before attempting quantitative comparisons are discussed in the concluding remarks.

B. Growth of planar films

Let us now show that the very same model also predicts the possibility to grow flat films by kinetically suppressing island formation. The evolution reported in Fig. 5 was obtained by decreasing the mobility by a factor 100 with respect to the

previous case [40], thereby mimicking the low-T growth stage used in experiments to stimulate dislocation injection prior to island growth [8,9].

The reduced mobility slows down the development of the ATG instability so that the film grows almost flat until it reaches the critical thickness for dislocation injection (around $\sim$1.2 nm with our parameters). When this occurs a first dislocation is introduced (an array of dislocations distanced by the cell size is actually introduced due to PBCs). Others follow at larger thicknesses. No islands are formed. As evident from the strain maps of Fig. 5, in these simulations we have considered 90° and not 60° dislocations. This is because in flat Ge/Si(001) films 60° dislocations tend to combine in 90° Lomer pairs [24,41]. Importantly, it is not the change in the defect character to cause the different behavior with respect to the close-to-equilibrium case: We directly verified (not shown) that the qualitative behavior is unchanged by replacing 60° (90°) dislocations with 90° (60°) dislocations in close-to-equilibrium (out-of-equilibrium) conditions.

Some undulations as also reported in the low-T experiments of Ref. [24] are seen in Fig. 5(a). Although they cause some roughening [panel (b)], they should not be confused with SK islands. They are indeed caused by the modulation in chemical potential induced by the presence of the dislocations. At variance with SK islands, such undulations are suppressed when the film is thick enough (leading to a uniform chemical potential at the free surface), and dislocations relax the misfit strain [42]. Under these conditions there is no further need for forming islands, and the kinetic constraints can be removed while growing a thicker flat film. This is precisely the strategy successfully used in typical experiments [8,9] where a high-T step (yielding better material quality) follows the low-T one. Our simulations confirm the validity of the approach in showing [Fig. 5(b)] that the film roughness is actually reduced upon annealing after dislocations are introduced.

Finally, we notice that also dislocation-induced undulations can be suppressed by reducing the temperature further. In that extreme regime diffusion would be totally frozen and our model would predict conformal growth. However, the validity of the approach would be questionable as monoatomic surface steps created by dislocations are not included in our model while known to influence the film roughness in the absence of surface diffusion [25].

IV. CONCLUSIONS

In this paper we have presented a continuum model able to predict the dynamical evolution of a lattice-mismatched system under the influence of both elastic and plastic relaxations. The approach allows one to reproduce several key experimental observations, such as (a) fast coarsening leading to depletion zones around islands hosting dislocations, (b) cyclic growth of dislocated islands, and (c) growth of flat plastically relaxed films by kinetic suppression of islanding. Importantly, this successful comparison was achieved by keeping the model minimal therefore facilitating the understanding of the main driving forces influencing heteroepitaxy in the presence of dislocations. However, including a proper treatment of surface-energy and elastic-constant anisotropies [43] or accounting for dynamical Si/Ge intermixing [44,45] would surely provide a more realistic description.

Finally, an extension to 3D is required before attempting any quantitative comparison with experiments, demanding for an improved definition of the model [46,47]. Furthermore, the additional description of the dislocation geometry could conveniently be tackled by coupling the present approach with a 3D dislocation dynamics code. This would open up the appealing possibility to develop a growth simulator yielding predictions on both morphology and defect distribution. As lattice-mismatched heteroepitaxy of semiconductors is nowadays widespread also in industrial environments, such a tool could be strongly beneficial for applications.

[1] I. Berbezier and A. Ronda, Surf. Sci. Rep. **64**, 47 (2009).
[2] L. Miglio and F. Montalenti, in *Silicon-Germanium (SiGe) Nanostructures*, edited by Y. Shiraki and N. Usami (Woodhead, Cambridge, U.K., 2011), pp. 211–246.
[3] F. Montalenti, D. Scopece, and L. Miglio, C. R. Phys. **14**, 542 (2013). .
[4] R. Bergamaschini, M. Salvalaglio, R. Backofen, A. Voigt, and F. Montalenti, Adv. Phys. X **1**, 331 (2016).
[5] E. A. Fitzgerald, Mater. Sci. Rep. **7**, 87 (1991).
[6] D. Leonard, M. Krishnamurthy, C. M. Reaves, S. P. Denbaars, and P. M. Petroff, Appl. Phys. Lett. **63**, 3203 (1993).
[7] Y. W. Mo, D. E. Savage, B. S. Swartzentruber, and M. G. Lagally, Phys. Rev. Lett. **65**, 1020 (1990).
[8] L. Colace, G. Masini, F. Galluzzi, G. Assanto, G. Capellini, L. Di Gaspare, E. Palange, and F. Evangelisti, Appl. Phys. Lett. **72**, 3175 (1998).
[9] A. Sakai, N. Taoka, O. Nakatsuka, S. Zaima, and Y. Yasuda, Appl. Phys. Lett. **86**, 221916 (2005).
[10] F. K. LeGoues, M. C. Reuter, J. Tersoff, M. Hammar, and R. M. Tromp, Phys. Rev. Lett. **73**, 300 (1994).
[11] R. Vincent, Philos. Mag. **19**, 1127 (1969).
[12] M. De Seta, G. Capellini, F. Evangelisti, and C. Spinella, J. Appl. Phys. **92**, 614 (2002).
[13] M. Stoffel, A. Rastelli, J. Tersoff, T. Merdzhanova, and O. G. Schmidt, Phys. Rev. B **74**, 155326 (2006).
[14] F. Boioli, R. Gatti, M. Grydlik, M. Brehm, F. Montalenti, and L. Miglio, Appl. Phys. Lett. **99**, 033106 (2011).
[15] A. Marzegalli, V. A. Zinovyev, F. Montalenti, A. Rastelli, M. Stoffel, T. Merdzhanova, O. G. Schmidt, and L. Miglio, Phys. Rev. Lett. **99**, 235505 (2007).
[16] P. Müller and R. Kern, Appl. Surf. Sci. **162–163**, 133 (2000).
[17] B. P. Uberuaga, M. Leskovar, A. P. Smith, H. Jónsson, and M. Olmstead, Phys. Rev. Lett. **84**, 2441 (2000).
[18] C.-H. Chiu and H. Gao, Mater. Res. Soc. Symp. Proc. **356**, 33 (1995).
[19] J.-N. Aqua, T. Frisch, and A. Verga, Phys. Rev. B **76**, 165319 (2007).

[20] G.-H. Lu and F. Liu, Phys. Rev. Lett. **94**, 176103 (2005).
[21] D. Scopece, F. Montalenti, and M. J. Beck, Phys. Rev. B **85**, 085312 (2012).
[22] J. P. Hirth and J. Lothe, *Theory of Dislocations*, 2nd ed. (Krieger, Malabar, FL, 1982).
[23] A. K. Head, Proc. Phys. Soc., London, Sect. B **66**, 793 (1953).
[24] A. Marzegalli, M. Brunetto, M. Salvalaglio, F. Montalenti, G. Nicotra, M. Scuderi, C. Spinella, M. De Seta, and G. Capellini, Phys. Rev. B **88**, 165418 (2013).
[25] A. M. Andrews, R. LeSar, M. A. Kerner, J. S. Speck, A. E. Romanov, A. L. Kolesnikova, M. Bobeth, and W. Pompe, J. Appl. Phys. **95**, 6032 (2004).
[26] J. D. Eshelby, Proc. R. Soc. London, Ser. A **241**, 376 (1957).
[27] T. Mura, *Mechanics of Elastic and Inelastic Solids*, 2nd ed., edited by S. Nemat-Nasser and G. A. Oravas, Mechanics of Elastic and Inelastic Solids Vol. 3 (Springer, Netherlands/ Dordrecht, 1987).
[28] E. Bonera, R. Gatti, G. Isella, G. Norga, A. Picco, E. Grilli, M. Guzzi, M. Texier, B. Pichaud, H. von Känel, and L. Miglio, Appl. Phys. Lett. **103**, 053104 (2013).
[29] R. Gatti, A. Marzegalli, V. A. Zinovyev, F. Montalenti, and L. Miglio, Phys. Rev. B **78**, 184104 (2008).
[30] M. Salvalaglio and F. Montalenti, J. Appl. Phys. **116**, 104306 (2014).
[31] W. Cai, A. Arsenlis, C. R. Weinberger, and V. V. Bulatov, J. Mech. Phys. Solids **54**, 561 (2006).
[32] R. Hull, in *Properties of Silicon Germanium and SiGe: Carbon*, edited by E. Kasper and K. Lyutovich (Inspec, Exeter, U.K., 2000), pp. 21–41.
[33] J. Alberty, C. Carstensen, S. A. Funken, and R. Klose, Computing **69**, 239 (2002).
[34] B. J. Spencer, P. W. Voorhees, and S. H. Davis, Phys. Rev. Lett. **67**, 3696 (1991).
[35] D. J. Godbey, J. V. Lill, J. Deppe, and K. D. Hobart, Appl. Phys. Lett. **65**, 711 (1994).
[36] Considering pure Ge requires a major meshing effort as both critical thicknesses for island formation and for dislocation injection are smaller. Use of a slightly lower misfit allowed us to handle more easily numerical stability while marginally altering results.
[37] R. J. Asaro and W. A. Tiller, Metall. Trans. **3**, 1789 (1972).
[38] M. A. Grinfeld, Sov. Phys. Dokl. **31**, 831 (1986).
[39] R. Gatti, F. Pezzoli, F. Boioli, F. Montalenti, and L. Miglio, J. Phys.: Condens. Matter **24**, 104018 (2012).
[40] The evolution predicted by our model depends only on the ratio between the mobility and the deposition flux. Decreasing one or increasing the other is therefore equivalent.
[41] Y. B. Bolkhovityanov, A. S. Deryabin, A. K. Gutakovskii, and L. V. Sokolov, Acta Mater. **61**, 617 (2013).
[42] E. A. Fitzgerald, Y.-H. Xie, D. Monroe, P. J. Silverman, J. M. Kuo, A. R. Kortan, F. A. Thiel, and B. E. Weir, J. Vac. Sci. Technol. B **10**, 1807 (1992).
[43] P. Liu, Y.-W. Zhang, and C. Lu, Appl. Phys. Lett. **88**, 041922 (2006).
[44] Y. Tu and J. Tersoff, Phys. Rev. Lett. **98**, 096103 (2007).
[45] R. Bergamaschini, J. Tersoff, Y. Tu, J. J. Zhang, G. Bauer, and F. Montalenti, Phys. Rev. Lett. **109**, 156101 (2012).
[46] Y.-W. Zhang, Phys. Rev. B **61**, 10388 (2000).
[47] M. Albani, R. Bergamaschini, and F. Montalenti, Phys. Rev. B **94**, 075303 (2016).